



Contents lists available at ScienceDirect

Annals of Nuclear Energy

journal homepage: www.elsevier.com/locate/anucene

Extension of ASTEC-Na capabilities for simulating reactivity effects in Sodium Cooled Fast Reactor



V. Matuzas^a, L. Ammirabile^{a,*}, L. Cloarec^b, D. Lemasson^c, S. Perez-Martin^d, A. Ponomarev^d

^aEuropean Commission Joint Research Centre (JRC), Directorate G – Nuclear Safety and Security, Westerduinweg 3, 1755LE Petten, The Netherlands

^bInstitut de Radioprotection et de Surete Nucleaire (IRSN), Saint-Paul-les-Durance, France

^cElectricite de France, R&D, 7 boulevard Gaspard Monge, France

^dKarlsruhe Institute of Technology (KIT), Institute for Neutron Physics and Reactor Technology, Hermann-von-Helmholtz-Platz 1, 76344 Eggenstein-Leopoldshafen, Germany

ARTICLE INFO

Article history:

Received 14 April 2017

Received in revised form 8 December 2017

Accepted 9 December 2017

Available online 26 December 2017

Keywords:

JASMIN project

Sodium-cooled Fast Reactors

Neutronic reactivity feedback

Unprotected flow coast-down

Severe accidents

ABSTRACT

The EU-JASMIN project (7th FP of EURATOM) has been centred on the development and validation of the new severe accident analysis code ASTEC-Na (Accident Source Term Evaluation Code) for Sodium-cooled Fast Reactors (SFR). The development of such computational tool being able to assist safety analysis of innovative reactor concepts is of crucial importance. One of the challenging issues when modelling SFRs is the neutronic reactivity feedbacks. This paper presents the model implemented in ASTEC-Na for representing the reactivity effects in SFR as well as the benchmarking results of a ULOF transient against SAS-SFR code results. It has been verified that the models are correctly implemented and that ASTEC-Na is now able to calculate reactivity feedbacks not only in the sodium single phase, but also after boiling onset and fuel in-pin relocation.

© 2017 The Authors. Published by Elsevier Ltd. This is an open access article under the CC BY-NC-ND license (<http://creativecommons.org/licenses/by-nc-nd/4.0/>).

1. Introduction

Within the JASMIN Collaborative Project (Joint Advanced Severe accidents Modelling and Integration for Na-cooled fast neutron reactors) supported by the 7th Euratom Framework Program, the new European severe accident analysis code for Sodium-cooled Fast Reactors (SFR), ASTEC-Na, has been further developed and assessed (The JASMIN).

The ASTEC-Na code aims at providing capabilities to evaluate the consequences of unprotected severe accidents including the source term evaluation (Girault and Van Dorselaere, 2013; Girault and Cloarec, 2015). The development performed so far was focused on the Initiating Phase of SFR severe accident sequence.

One of the challenging elements in such analyses is the reactivity feedback model. In order to extend ASTEC-Na capabilities in the SFR analysis domain, one of the work packages of the JASMIN project was devoted to the development and implementation of neutron physics feedback modelling capabilities.

Initially the development of a Point Kinetics model in the ASTEC-Na code was based on the one available in the IRSN SCA-

NAIR code (Moal et al., 2014). As this model was dedicated to the neutron physics feedback reactivity computation for the LWR fuel pin tests in the CABRI facility, a more generic reactivity feedback model (so called 'LOCAL' model) using coefficients related to temperature variation (pcm/K) had been implemented. Such approach is acceptable only until sodium boiling or material relocation starts. For modelling fuel and cladding relocation reactivity feedbacks, as well as the sodium void reactivity effect, it has been necessary to develop a new approach for the assessment of the reactivity feedbacks. By changing the reactivity feedback model based on temperature variation to mass variation, ASTEC-Na neutron physics model (so called 'LOCALM') is able to cope with post boiling phenomena. More specifically, the latest ASTEC-Na model LOCALM is able to predict reactivity evolution resulting from sodium boiling, and in-pin molten fuel motion.

This paper is structured as follows: after the description of the neutron reactivity model implemented in ASTEC-Na in Section 2, a description of the benchmark exercise performed in JASMIN WP2.4 for assessing the new ASTEC-Na model is presented in Section 3. This benchmark exercise consisted in the simulation of an Unprotected Loss of Flow (ULOF) accident using the SFR core design studied in the European project CP-ESFR (Collaborative Project for a European Sodium Fast Reactor). The project (Fiorini and Vasile, 2011) was performed (2009–2012) in the 7th European Framework Programme and was devoted to the identification and study of innovations to be considered for the future in the core

* Corresponding author at: European Commission Joint Research Centre (JRC), Directorate G – Nuclear Safety and Security, Westerduinweg 3, 1755LE Petten, The Netherlands.

E-mail address: luca.ammirabile@ec.europa.eu (L. Ammirabile).

design, safety, reactor architecture, components and the dissemination of knowledge related to this technology. Code modellings as used by ASTEC-Na and SAS-SFR codes are described in Section 4. Benchmarking results against SAS-SFR code are presented in Section 5 and the final conclusions of the work performed in the JASMIN project concerning the performance of the ASTEC-Na neutron reactivity model are given in Section 6.

2. Neutron physics model implementation in ASTEC-NA

The general neutron reactivity model implemented in ASTEC-Na is based on the Point Kinetics model. The main assumption is that the reactor is close to equilibrium, so that the neutron flux can be divided into two components: a time component $P(t)$ and a space and energy term $\varphi(r, E)$. Therefore, the flux shape and spectrum do not evolve with time. This hypothesis is valid only if the perturbation of the core remains limited. Point Kinetics is often restricted to the study of the primary phase of severe accidents, the transition phase of transients being totally out of its scope. One should keep in mind however, that even during the primary phase, material relocation can disturb flux shape (fuel relocation for example) and spectrum (sodium voiding for example). Point Kinetics should not be considered as a reference hypothesis but as a convenient solution to investigate severe accidents at low development and computation costs.

The evolution of the time component of power is controlled by $n_g + 1$ equations: n_g equations for the fission power triggered by neutron from precursors, and one equation for the neutron physics power evolution:

$$\begin{cases} \frac{dP(t)}{dt} = \frac{\rho(t) - \beta}{\Lambda} P(t) + \sum_{i=1}^{n_g} \lambda_i C_i(t) \\ \frac{dC_i(t)}{dt} = -\lambda_i C_i(t) + \frac{\beta_i}{\Lambda} P(t) \end{cases} \quad i = 1, n_g \quad (1)$$

where:

- t = time (s)
- $P(t)$ = neutronic power (W)
- $\rho(t)$ = total reactivity
- $C_i(t)$ = fission power triggered by neutron from precursors i (W)
- β_i = fraction of delayed neutrons of group i
- $\beta = \sum_{i=1}^{n_g} \beta_i$ = fraction of delayed neutrons
- Λ = mean generation time of neutrons (s)
- λ_i = decay constant of group i precursors (s^{-1})

With t_0 defined as the beginning of transient, the reactor is at neutron physics and thermal equilibrium (steady-state conditions) for $t \leq t_0$:

$$\rho(t_0) = 0. \quad P(t_0) = P_0 \quad C_i(t_0) = \frac{\beta_i}{\lambda_i \Lambda} P(t_0) \quad (2)$$

The total reactivity $\rho(t)$ is the sum of external reactivity injected ($\rho_{ext}(t)$, defined by the user), reactivity contributions from control rods ($\rho_R(t)$, defined by the user) and reactivity feedbacks ($\rho_{FB}(t)$, computed by the code):

$$\rho(t) = \rho_{ext}(t) + \rho_R(t) + \rho_{FB}(t) \quad (3)$$

The $\rho_{FB}(t)$ takes into account five reactivity feedbacks $\rho_x(t)$ with x belonging to the five reactivity effects listed below for each model.

For model LOCAL (Fig. 1):

- Doppler effect;
- Fuel reactivity effect (fuel axial expansion);
- Cladding reactivity effect (cladding axial and radial expansion);

- Wrapper reactivity effect (wrapper axial and radial expansion);
- Sodium reactivity effect (sodium density variation).

For the LOCAL model, fuel and cladding axial expansions are computed with their respective temperatures. Therefore, a free expansion of the fuel column and cladding is supposed. This hypothesis is valid for fresh fuel or if a cooling down of the fuel is experienced. This can be the case during Unprotected Loss Of Flow transients in low void effect Sodium Fast Reactors: coolant temperature, and therefore cladding temperature increase while power reduces significantly. The fuel temperature can then go down and the fuel contraction can re-open the gap between pellet and cladding, so free axial expansion can occur.

For model LOCALM (Fig. 2):

- Doppler effect;
- Fuel reactivity effect (fuel axial expansion and fuel in-pin relocation);
- Cladding reactivity effect (cladding axial expansion);
- Wrapper reactivity effect (wrapper axial expansion);
- Sodium reactivity effect (which includes sodium density variation, sodium voiding, as well as cladding and wrapper radial expansion).

Contrary to the LOCAL model, the LOCALM model is not based on temperature variations but on mass distribution evolution. Therefore, the reactivity model can deal with cladding-controlled, force balance controlled or free axial expansion of cladding and fuel, depending on the thermal-mechanical model governing axial expansion of the pin.

A more detailed description of the actual model of LOCALM is provided hereafter.

As implemented in the code, an area a is identified as a group of axial meshes in a channel with the same local feedback coefficients. The variation in mass is calculated for each macro-component (fuel, cladding, wrapper tube) and sodium in each area. If some components are extending out of geometrical initial areas, these masses are taken into account using the coefficients of the area just below. The main issue in this formulation is the correct calculation of the mass of fuel, cladding, wrapper tube and sodium present at each time in each axial region, taking into account the mass evolution due to sodium, fuel, wrapper tube and cladding axial expansion as well as in-pin fuel relocation.

Diagrid effect and relative axial dilatation between control rods and vessel are not yet modelled in ASTEC-Na but it is planned to take them into account in the future. Sodium inter-assembly effect can currently only be computed if the inter-assembly gap is modelled in the input data.

2.1. Doppler effect

For Doppler reactivity the following equation is applied:

$$\rho_D^a(t) = K_D(a, t) * \ln \left(\frac{T_{fuel}^a(t)}{T_{fuel}^a(t_0)} \right) * \frac{m_{fuel}^a(t)}{m_{fuel}^a(t_0)} \quad (4)$$

where $K_D(a, t)$ is the local Doppler coefficient in the area a at time t , $T_{fuel}^a(t)$ is the mass-averaged fuel macro-component temperature (in K) in the area a at time t ; $T_{fuel}^a(t_0)$ is the mass-averaged temperature at initial time t_0 in area a ; and $m_{fuel}^a(t)$ and $m_{fuel}^a(t_0)$ are the masses of fuel present in the area a at time t and time t_0 , respectively.¹

¹ Fuel macroscopic absorption section is proportional to fuel mass. In a first approximation the Doppler reactivity effect is considered proportional to fuel mass during in-pin relocation.

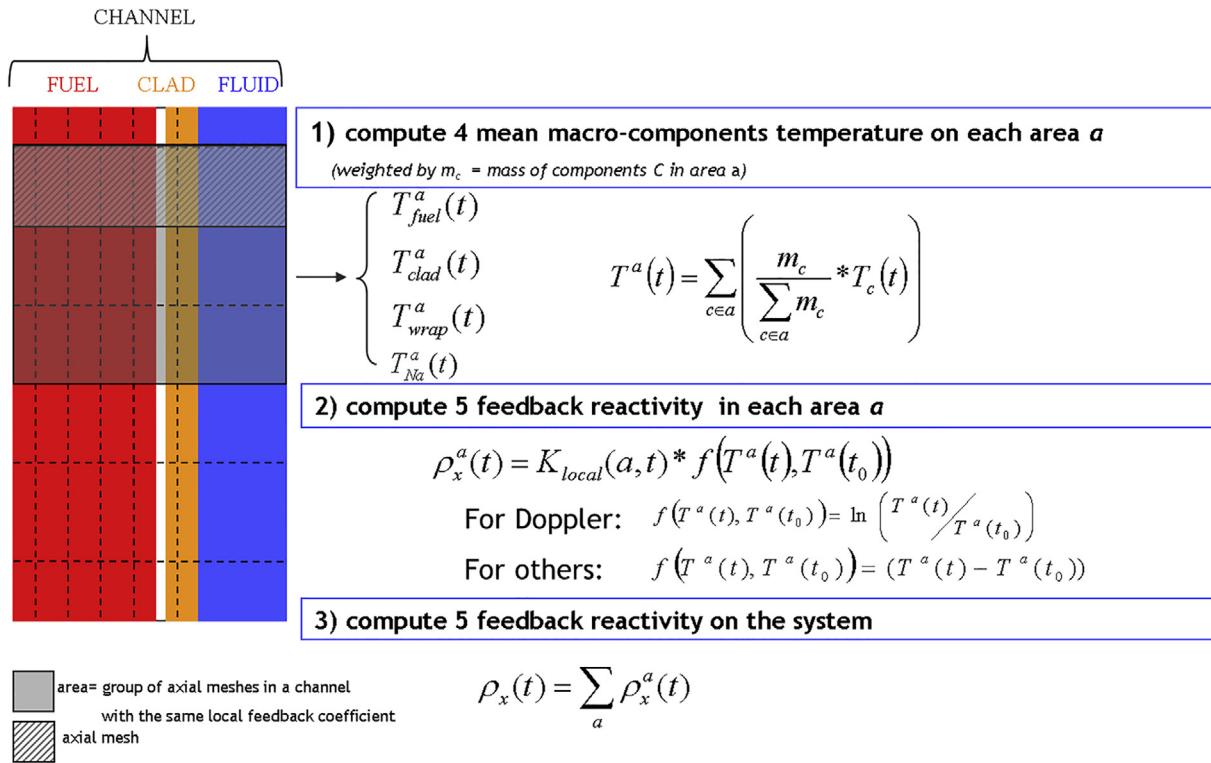


Fig. 1. Feedback reactivity computation with model 'LOCAL'.

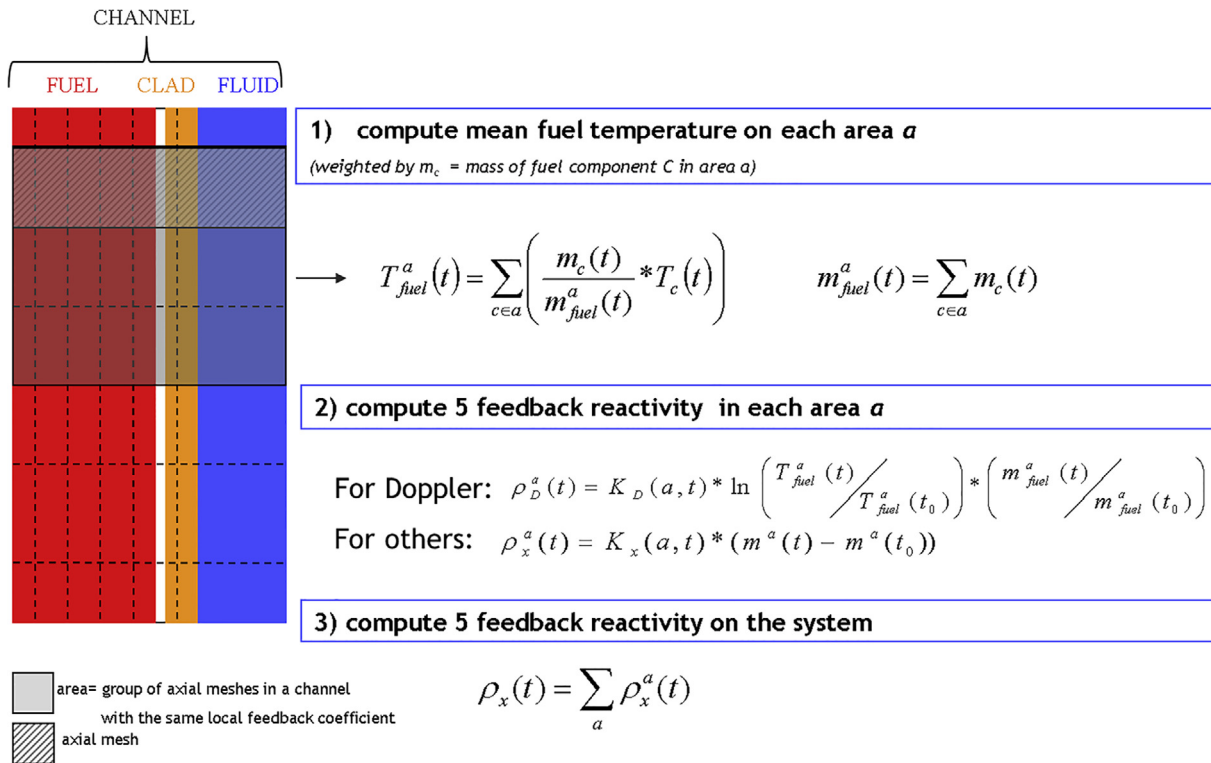


Fig. 2. Feedback reactivity computation with model LOCALM.

After boiling onset, the Doppler coefficient $K_D(a, t)$ will be calculated as follows:

$$K_D(a, t) = \alpha_{Na}(a, t) * K_D^{void}(a, t) + (1 - \alpha_{Na}(a, t)) * K_D^{nom}(a, t) \quad (5)$$

where $K_D^{void}(a, t)$ and $K_D^{nom}(a, t)$ are the Doppler contribution in voided and nominal sodium conditions respectively and $\alpha_{Na}(a, t)$ is sodium void fraction in the area a at time t .

2.2. Fuel reactivity effect

The fuel reactivity effect is defined as the reactivity change due to the variation of fuel mass in area a . In the proposed model, the following equation is applied for fuel reactivity effect:

$$\rho_{fuel}^a(t) = K_{fuel}(a, t) * (m_{fuel}^a(t) - m_{fuel}^a(t_0)) \quad (6)$$

where $K_{fuel}(a, t)$ is the spatial distribution of the fuel reactivity coefficient, and $m_{fuel}^a(t)$ and $m_{fuel}^a(t_0)$ are the masses of fuel present in the area a at time t and time t_0 respectively.

2.3. Cladding reactivity effect

The cladding reactivity effect is defined as the reactivity change due to the variation of cladding mass in the area. Similar as for fuel reactivity feedback, the new cladding reactivity effect is calculated by:

$$\rho_{clad}^a(t) = K_{clad}(a, t) * (m_{clad}^a(t) - m_{clad}^a(t_0)) \quad (7)$$

where $K_{clad}(a, t)$ is the spatial distribution of the cladding reactivity coefficient, and $m_{clad}^a(t)$ and $m_{clad}^a(t_0)$ are the masses of cladding present in the area a at time t and time t_0 , respectively.

2.4. Wrapper tube reactivity effect

The wrapper tube reactivity effect is defined as the reactivity change due to the variation of wrapper tube mass in the area. In this case, the following equation is applied for the wrapper tube reactivity effect:

$$\rho_{wrap}^a(t) = K_{wrap}(a, t) * (m_{wrap}^a(t) - m_{wrap}^a(t_0)) \quad (8)$$

where $K_{wrap}(a, t)$ is the spatial distribution of the wrapper tube reactivity coefficient, and $m_{wrap}^a(t)$ and $m_{wrap}^a(t_0)$ are the masses of wrapper tube present in the area a at time t and time t_0 , respectively.

2.5. Sodium reactivity effect

The sodium reactivity effect is defined as the reactivity change due to the variation of sodium mass in the area. For sodium reactivity effect the following equation is applied:

$$\rho_{Na}^a(t) = K_{Na}(a, t) * (m_{Na}^a(t) - m_{Na}^a(t_0)) \quad (9)$$

where $K_{Na}(a, t)$ is the spatial distribution of the sodium reactivity coefficient, and $m_{Na}^a(t)$ and $m_{Na}^a(t_0)$ are the masses of sodium present in the area a at time t and time t_0 , respectively.²

This expression takes into account the effect of cladding and wrapper tube radial expansion in pushing away the sodium coolant from the axial region. In fact the radial expansion is considered within the fluid feedback effect by changing assembly and inter-assembly fluid channels geometries.

² This is a first approximation considering that sodium reactivity can be strongly non-linear with mass variation in regions near core boundaries.

2.6. Total reactivity feedback

The total reactivity feedback of the system at time t will then be computed summing up the different region contributions of all reactivity feedbacks:

$$\rho_{FB}(t) = \sum_x \sum_a \rho_x^a(t) \quad (10)$$

where a represents the areas meshing and x the individual reactivity feedbacks considered (fuel, cladding, wrapper tube, sodium and Doppler). For numerical purposes it is convenient to sum up together all contributions at time t and all contributions at time t_0 separately:

$$\rho_{FB}(t) = \sum_x \left(\sum_a K(a, t) * m_x^a(t) - \sum_a K(a, t) * m_x^a(t_0) \right) + \left(\sum_a K_D(a, t) * \ln(T_{fuel}^a(t)) * \frac{m_{fuel}^a(t)}{m_{fuel}^a(t_0)} - \sum_z K_D(a, t) * \ln(T_{fuel}^a(t_0)) * \frac{m_{fuel}^a(t)}{m_{fuel}^a(t_0)} \right) \quad (11)$$

Notice: As can be seen in Eqs. (4)–(11), ASTEC-Na neutronics model has been structured to be easily extended to time-dependent reactivity coefficients so as to overcome the limitations expressed at the beginning of this paragraph. Reactivity coefficients could then be updated each time the situation is too far from the configuration in which they were computed, so as to always remain in a low perturbation hypothesis. A good strategy of updating frequency would then be necessary to optimize the precision over computation time ratio.

3. Benchmark exercise

The scope of the benchmark exercise is to compare the actually implemented neutron physics capabilities of ASTEC-Na with the capability of other current severe accident code, the SAS-SFR code (Imke and Struwe, 1994; Kruessmann et al., 2015; Genshiryoku and Kiban, 2011), to simulate the initiation phase of an unprotected loss of flow accident (ULOF) in a pool-type sodium-cooled fast reactor. The ULOF accident is one of the enveloping cases for the consequence of postulated severe accidents in SFR and the neutron physics feedback plays a crucial role in the transient. Hence the insights of the benchmark can be usefully extrapolated to other scenarios under the domain of validity of the Point Kinetics model. As a benchmark reactor model serves the “Reference Oxide core design” concept of the CP-ESFR project under Beginning of Life (BOL) core load conditions (Blanchet and Buiron, 2009; Rineiski et al., 2011). A simplified representation of the reactor core was employed.

The accident is initiated by the failure of all primary pumps without activation of the reactor shutdown systems leading to a subsequent decrease of the coolant flow in the core. Due to the diverse and redundant design of the shutdown system, the probability of such an accident is extremely low. In addition, in most of the cases the inertia of flywheels attached to the primary pump power supply system could impede a fast decrease of the coolant flow. The flow coast down rate plays an important role for the further progression of the accident. In this benchmark the coolant flow rate decreases rapidly due to the short coolant flow halving time of 10 s, provoking a fast undercooling of the core. The reduction in power generation develops much slower so that the power-to-flow ratio mismatch results in a subsequent rapid single phase coolant heat-up which may lead to coolant boiling, cladding dry-out, cladding melting and relocation, and subsequent fuel pin break-up followed by core materials relocation.

Table 1
ESFR nominal characteristics.

Reactor power (MWth)	3600
Core inlet temperature (°C)	395
Core outlet temperature (°C)	545
Average core structure temperature (°C)	470
Average fuel temperature (°C)	1227

Table 2
ESFR oxide fuel subassembly characteristics.

Number of subassemblies in the core	225 (inner core) 228 (outer core)
Subassemblies pitch (mm)	210.8
Sodium gap width inter assembly (mm)	4.5
Wrapper tube outer flat-flat width (mm)	206.3
Wrapper tube thickness (mm)	4.5
Wrapper tube material	FM steel (EM10)
Wire wrap spacer diameter (mm)	1.0
Wire wrap helical pitch (mm)	225
Wire wrap spacer material	15/15Ti steel
Outer cladding diameter (mm)	10.73
Inner cladding diameter (mm)	9.73
Cladding material	15/15Ti steel
Fuel pellet diameter (mm)	9.43
Fuel pellet hole diameter (mm)	2.5
Fuel pellet material	(U, Pu)O ₂
Fuel average density	88.8% TD
Fuel porosity	4.5%
O/M	1.98

Table 3
ESFR core channel grouping.

Channel group	Number of SA	Average SA power (MW)	Total Power fraction	Linear power PPN ¹ (W/cm)
1	30	6.64	5.6%	293.60
2	48	7.04	9.5%	311.10
3	63	7.56	13.3%	333.20
4	84	8.02	18.8%	353.20
5	6	11.00	1.8%	481.50
6	30	10.34	8.7%	453.10
7	84	9.33	21.9%	409.60
8	42	7.90	9.3%	347.90
9	30	6.79	5.7%	300.00
10	36	5.38	5.4%	238.40

(U, Pu)O₂ pellets in 15/15Ti steel cladding, upper and lower dummy axial blankets and fission gas plena. In each subassembly, a sodium plenum of 15.1 cm height is located on top of the pins (it was not considered in the modelling). The hexagonal wrapper tubes are made of ferritic martensitic steel (EM10).

The geometry modelled in the benchmark was limited to the pin length. Simplified axial reactor core layout is given in Fig. 3.

In order to account for the radial and axial variation in power and flow characteristics of a reactor core, severe accident codes employ the concept of channels which consist of subassembly groups with similar thermal-hydraulics, neutron physics and fuel pin mechanics behaviour. Subassemblies in the same channel are considered to behave identically. The grouping used for the ESFR core is presented in Table 3 where 9 channels (1–4 and 6–10) represent cooling groups and one channel (number 5) represents the 6 subassemblies (SAs) with the highest power in the core.

3.1. Peak power node

For the purpose of the benchmark the same axial normalized power profile was assumed in all channels. The nominal coolant mass flow rate per channel had to be adjusted in each simulation to achieve the coolant heat-up of 150 °C across the channel. In SAS-SFR, the required mass flow rates are input and inlet pressure drop coefficients in each channel are adjusted automatically by the code to fit core inlet and outlet pressure specifications.

The ULOF transient considered in the benchmark exercise is assumed to start at full power operation with the failure of all shutdown systems and all primary coolant pumps. Then the coolant flow rate is assumed to decay with halving time of 10 s following the equation:

$$Q(t) = Q_0 \frac{1}{1 + \frac{t}{10}} \quad (12)$$

where Q_0 is the nominal mass flow rate.

As a first approximation, the core inlet temperature and outlet pressure are assumed constant during the transient respectively at 395 °C and 2 bar.

The core reactivity behaviour, issued from KANEXT and used for SAS-SFR and ASTEC-Na models, is described using axial and radial discretization schemes of the whole core by defining various reactivity effects along the height of the core (layer-wise) and along the core cross section (group-wise). For the pin height only reactivity feedbacks for the lower axial blanket (3 layers), fissile core (13 layers), upper axial blanket (2 layers) and upper fission gas plenum (1 layer) are considered. Radial discretisation considers 8 feedback groups allocated as coaxial rings. The reactivity effects are considered to be the same for all subassemblies of one feedback group, and all subassemblies in a group have the same axial distribution of effects. Channel groups 5, 6 and 7 use the same reactivity group, while the rest of the channel groups are assigned to a specific reactivity group.

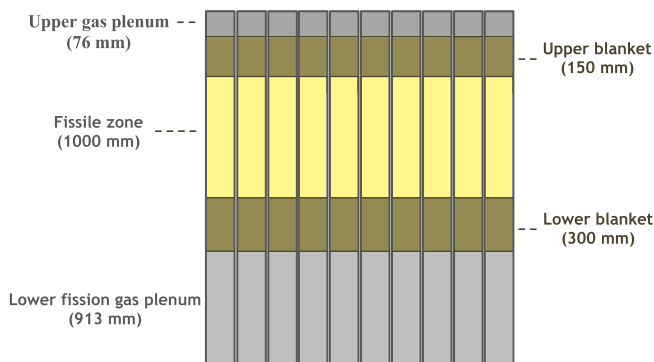


Fig. 3. Simplified axial reactor core layout (with indicated cold dimensions).

Moreover, the increase in the coolant and fuel temperature induces variations of the associated reactivity feedbacks which considerably determine the course of the ULOF transient. In the initiation phase of a ULOF accident, reactivity feedbacks due to the fuel Doppler reactivity, the coolant expansion and voiding, the fuel axial expansion and the initial fuel dispersion play a determining role. The benchmark analysis is divided into two phases:

- The first phase of the ULOF simulation covers the single phase coolant heat-up up to coolant boiling onset.
- The second phase deals with the boiling phase of the transient up to the occurrence of first fuel pin failure.

This ULOF specification is based on the SAS-SFR analysis performed in the CP-ESFR project where the neutron physics calculations providing the power profiles and the reactivity coefficients were done with KANEXT code (Dagan et al., 2004; KANEXT).

The ESFR nominal characteristics are summarised in Table 1 and oxide fuel subassembly characteristics in Table 2. Each fuel subassembly contains 271 fuel pins with helical wire wrap spacers in a hexagonal wrapper tube. The fuel pellet diameter is 9.43 mm and the cladding thickness is 0.5 mm. The fuel pin consists of

4. Modelling

For the benchmark exercise one ASTEC-Na model and two SAS-SFR models (referred as SAS-SFR (1) and SAS-SFR (2) further in the paper) have been developed according to the benchmark specifications. For preparation of SAS-SFR models two independent groups have been involved. As the same specifications was considered, these two SAS-SFR simulations will enable to estimate the impact of the user effect on results and thus will help to evaluate whether differences to results obtained with ASTEC-Na are of importance. The following sections provide an overview of the models developed.

4.1. ASTEC-Na model

For the benchmark exercise a model of the ESRF “Reference Oxide core design” has been developed by using the latest version of ASTEC-Na v2.1.

Following the benchmark specifications, the reactor is described in a simplified manner. The primary circuit is not explicitly modelled. The model was made using two ASTEC-Na modules – CESAR and ICARE. The cold plenum (VBOT) as well as the hot plenum (VTOP) is represented by a single CESAR volume. The SFR core is represented using ICARE.

A constant temperature sodium (395 °C) injection is simulated directly into the volume VBOT by a pump at a constant rate and the sodium is removed from the volume VTOP (break in the top volume). The core consists of 453 subassemblies (SA) grouped into 10 channel groups. Each channel group is modelled in ASTEC-Na using CHANNEL structure, with the cross-section corresponding to overall cross-section of the corresponding SA group. Inlet of each SA group is directly connected to the VBOT volume and outlet to the VTOP volume (Fig. 4).

Each SA group has individual power and sodium mass flow rate values. The total core power is 3600 MWth and it was distributed among SA channel groups according to power fractions indicated in Table 3. The inter-assembly channels are not considered in the model. The power is produced only in the fissile fuel part. The axial fuel pin power profile has a cosine-like shape set according to benchmark specifications and for radial fuel pin power uniform distribution is assumed.

The total sodium mass flow rate of 18906.5 kg/s is imposed at the VBOT inlet. Similarly to SAS-SFR the inlet pressure drop coefficients in each channel are tuned to define the reference value for the sodium mass flow per channel group so that the coolant heat-up along the simulated pin is 150 °C (target outlet temperature of 545 °C). The coolant exit pressure is set to 2.0 bar constantly during the transient and the coolant inlet temperature is set to

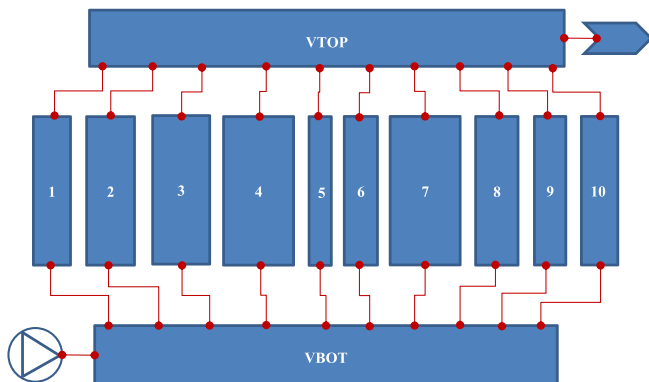


Fig. 4. ASTEC-Na model.

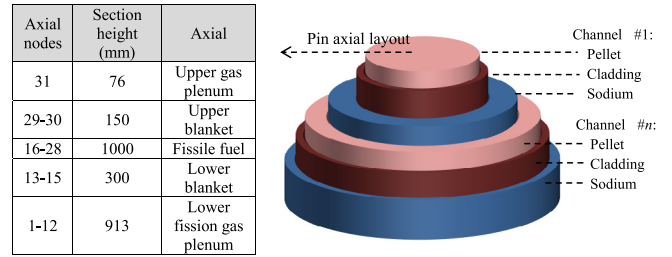


Fig. 5. Layout of core SA groups.

668.15 K (395 °C). No coolant by-pass is assumed and all sodium passes through the core.

The main thermal-hydraulic data concerning the steady-state conditions before the transient phase are summarised in Section 5.1. The initial conditions at the beginning of the transient are stabilized through a steady-state calculations lasting 200 s.

The model discretisation was made of 31 axial meshes, 10 radial meshes of equal masses for pellets and blankets (except inner and outer meshes, which was half-sized) and 5 radial meshes for cladding (uniformly distributed radially). The core itself was modelled as a set of concentric cylinders (Fig. 5). Each cylinder represented a single SA group (pellet/cladding) and its sodium channel. The wrapper is not considered in the model.

Reactivity feedbacks considered in ASTEC-Na calculation are the ones described in Section 2, except the wrapper tube effect as it is not modelled in ASTEC-Na input data: Doppler (distinguishing between liquid channel conditions and full voided channel conditions), coolant density and void reactivity, cladding and fuel axial expansion and cladding and fuel material relocation feedbacks. As defined in the benchmark specifications the effect of the heat-up of the inter-assembly sodium is not considered in this exercise.

In this paper, a distinction is made between sodium density effect and sodium voiding effect on reactivity. Even if both are linked to the variation of the number of sodium atoms in a volume, the impact on the reactivity of a core with a sodium plenum is very different whether the sodium density is close to nominal (sodium thermal expansion) or almost null (sodium voiding). In a reactivity feedback model using only one set of sodium reactivity coefficients, the results would be very different whether the coefficients are computed with a small perturbation of the sodium density or with a complete voiding of the core.

The kinetics parameters for beginning-of-life (BOL) were used in accordance with the benchmark specifications. The prompt neutron generation time was set to 0.495 μs and 6 groups of delayed neutron precursor families have been used (Table 4).

In ASTEC-Na calculations using LOCALM, the advanced model named RIA has been deployed to simulate the thermo-mechanical behaviour of fuel and cladding during a reactivity-initiated accident. This RIA model implemented in ICARE for computing the fuel thermo-mechanics is based on the fuel safety analysis code SCANAIR LWR (where cladding post-failure events are not modelled) developed for Reactivity Insertion Accident (RIA) transients and extended to SFR (Cloarec and Moal, 2012). Different aspects of RIA models were greatly improved and benchmarked during the JASMIN project. However, it should be noted that some of the RIA submodels, not fully validated, still show some deficiencies in correctly predicting both the axial fuel expansion and the cladding deformation by pellet-cladding mechanical interaction (PCMI) and these have to be taken into account during interpretation of neutron physics benchmarking results.

The characteristics of cladding material (expansion coefficient, thermal capacity, thermal conductivity) are set in ASTEC-Na as close as possible to the ones available in SAS-SFR. For fuel physical properties, (density, specific heat and melting temperatures) the

Table 4
Kinetics data of ESFR Reference Oxide core at BOL state.

	Group 1	Group 2	Group 3	Group 4	Group 5	Group 6
Yield β_i	$8.169 \cdot 10^{-5}$	$7.313 \cdot 10^{-4}$	$6.224 \cdot 10^{-4}$	$1.439 \cdot 10^{-3}$	$7.547 \cdot 10^{-4}$	$2.567 \cdot 10^{-4}$
Relative yield β_i/β	0.021	0.188	0.160	0.370	0.194	0.066
Decay constant λ_i , 1/s	0.0127	0.032	0.128	0.304	1.35	3.63

suggested options for MOX physical laws are selected. The fuel thermal conductivity is calculated based on the Philliponneau correlation. As-fabricated porosity value of 4.5% has been used. A constant 1.98 value of the oxygen to metal ratio of the fuel to be used for the calculation of the thermal conductivity has been used. The recommended correlations for MOX fuel thermal properties and SFR cladding failure models have been used (Cloarec and Moal, 2012), and the in-pin fuel relocation model (FOAM) has been activated.

Two methods are available in ASTEC-Na to compute fuel-cladding gap heat transfer. In the simplified standard method (without using RIA models), the fuel-cladding contact is assumed to be ideal (no surface roughness), although a contact resistance can be provided. The elaborated RIA gap heat transfer method considers conduction, radiation, convection and solid-solid contact. In the latter, the thermal inertia of the gases in the gap is neglected implying the heat fluxes from fuel to gas and from gas to cladding are equal. The radiative power from fuel to cladding is expressed by the Stefan-Boltzmann law considering fuel and cladding surface emissivity coefficients. As for the solid-solid heat exchange, two options are available, the mechanistic approach and the perfect contact approach. In the first approach the gap heat flux is the sum of the part transmitted through the gas pockets in the surface roughness and the part transmitted directly via the two solid zones in contact. The second approach considers that the thermal contact is perfect without gas pocket contribution. For the neutron physics benchmark exercise the mechanistic approach has been selected to compute fuel-cladding gap heat transfer. This gap model allows to compute gap heat transfer whereas gap is open or closed. The solid-solid contact heat transfer with gas pockets is only assumed when the gap is really closed, not when it is open.

4.2. SAS-SFR models

The SAS-SFR code is a system code which performs deterministic analysis for steady-state power operation and the initiation phase of accidental transients in Sodium-cooled Fast Reactors. It is a version of the SAS4A code originally developed by Argonne National Laboratory (Cahalan et al., 1994; Wider et al., 1982; Hill, 1985) that has been jointly modified and maintained by KIT/INR (Germany), CEA, IRSN (France), and JAEA (Japan). Besides the development of SAS4 code, SAS-SFR accumulates the experience of about 400 person years. It has been validated successfully on results of the different CABRI experimental programmes (Perez-Martin and Pfrang, 2016; Perez-Martin and Pfrang, 2015).

As in the case of ASTEC-Na, the reactor is described in a simplified manner. The primary circuit is not explicitly modelled and the steady-state boundary conditions (temperatures, pressures) are set at pin extremities. Subassembly grouping into channels respects specifications of Table 3.

The axial discretisation of the SA is modelled in SAS-SFR with the pin zone comprising fissile and fertile fuel column and the fission gas plena. The pin section is divided into 5 sections: lower gas plenum with 5 axial nodes, lower fertile fuel with 3 axial nodes, fissile column with 13 axial nodes, upper fertile fuel with 2 axial nodes and the upper gas plenum with 1 axial node. The number of radial temperature nodes is 11 for the fuel. For the cladding, SAS-SFR uses 2 radial nodes with the same width. As for the clad-

ding temperature, it provides three values associated to the inner surface, midpoint and outer surface by using a linear interpolation.

The number of subassemblies for every channel is specified according to Table 3. The 271 pins per subassembly are represented in SAS-SFR as an average single pin. The thermal inertia of the wrapper is simulated using a slab geometry, i.e. a rectangle with one side defining the perimeter wetted by coolant and a thickness is chosen such that the cross-sectional area of the wrapper is kept.

The total power is 3600 MWth, however the fraction of total reactor power represented by sum of all SAS-SFR channels is 99.34% where only negligible amounts are assumed to be produced in cladding structure and coolant.

The axial fuel pin power profile has a cosine-like shape set according to benchmark specifications and the radial fuel pin power shape is set flat as for the case of a fast spectrum.

The energy per fission is set to 209.7 MeV. This value depends to some degree on the fuel composition and the neutron spectrum. Prompt neutron generation time is 0.495 μ s and the number of delayed neutron precursor families is set to 6 where the corresponding values are in accordance to benchmark specifications (Table 4).

Reactivity feedbacks considered in SAS-SFR calculation are the Doppler (distinguishing between liquid channel conditions and fully voided channel conditions), coolant density and void reactivity (two sets of coefficients are used: one computed with a low perturbation, one with a complete voiding of the core; a linear combination of both sets on sodium density is used), cladding and fuel axial expansion and cladding and fuel material relocation feedbacks. As defined in the benchmark specifications, the neutron physics feedback effect of the heat-up of the inter-wrapper sodium is not considered in this exercise, nor is the axial expansion of the hexcan. No control rod relative axial expansion has been modelled for this benchmark since ASTEC-Na was not able to deal with this feedback at the time of the benchmark.

PRIMAR-1 is the simplified module selected for this calculation where the coolant flow is specified as a function of time in the input. The reference value for the coolant mass flow per pin is selected so that the coolant heat-up along the simulated pin is 150 °C. The coolant exit pressure is set to 2.0 bar constantly during the transient and the coolant inlet temperature is set to 668.15 K (395 °C). No coolant by-pass is assumed and all sodium passes through the core. The basic equation used in SAS-SFR to compute the mass flow and pressure drop is the following:

$$\frac{1}{A} \frac{dw}{dt} + \frac{dp}{dz} + \frac{1}{A} \frac{d(wv)}{dz} = - \left(\frac{dp}{dz} \right)_{fr} - \left(\frac{dp}{dz} \right)_K - \rho g \quad (13)$$

where the friction and orifice pressure drops and the gravity head are considered. Orifice coefficients are defined for upward and downward flows in order to compute the pressure drops along the simulated pin region in normal and abnormal operation. The equations from V. Bessiron (Bessiron, 1998) are used for the sodium equation of state.

The sodium voiding model is a multiple-bubble slug ejection model that handles flow area changes and non-uniform axial nodes. It simulates the axial distribution of the voiding extent (for calculating the voiding reactivity feedback), the heat removal from the cladding surface after the onset of voiding and the vapour flow rates that drive the molten cladding motion. In the multi-

bubble model an upper sodium plenum is always assumed, therefore even though it was agreed in the benchmark to take into account only the SA regions, SAS-SFR code included an upper sodium plenum to handle two-phase sodium ejection and back-flow for jugging phenomena during boiling.

The recommendations included in the SAS-SFR input manual regarding the options and parameters of the fuel pin models are selected and the dynamic calculation of DEFORM module is activated. For fuel physical properties, (density, specific heat and melting temperatures) the suggested option for physical laws is selected. The fuel thermal conductivity is calculated based on the Philliponneau correlation. Two SAS-SFR calculations used slightly different as-fabricated porosity values – in the SAS-SFR (1) model 4.5% has been used and SAS-SFR (2) was set to 5%. With regard to the oxygen to metal ratio of the fuel to be used for the calculation of the thermal conductivity and burn-up dependence, both SAS-SFR models have used as initial value 1.98. However, SAS-SFR (2) has additionally used a model enabling computation of the stoichiometry imbalance redistribution taking into account oxygen migration from the center of the pellet to the surface (i.e. O/M ratio varies from 1.95 to 2.0).

The fuel-cladding gap conductance selected uses the standard URGAP-model which is the reference for experimental qualifications at steady-state and during transients considering not only the gap width, but also the inventory of fission gas release to plena and fuel-cladding gap and the fuel and cladding surface roughness when gap is closed.

Cladding physical properties (cladding density, thermal conductivity, specific heat and melting temperatures) as well as cladding yield stress, ultimate tensile strength and uniform elongation are calculated in SAS-SFR using the available option for 15–15 Ti cladding material model, based on experimental results obtained during the material tests performed within the CABRI programmes (Papin et al., 1996).

5. Simulation and benchmark results

5.1. Steady-state

The main goal of the steady-state calculations is to ensure that initial benchmark conditions among ASTEC-Na and SAS-SFR before the beginning of the transient are as close as possible. Before proceeding with the transient simulations different steady-state parameters were compared among different models. Values of the main steady-state SAS-SFR and ASTEC-Na parameters are summarised in Table 5.

As can be seen from the Table 5 the steady-state values are in good agreement among different simulations. Considering the different fuel models, SAS-SFR and ASTEC-Na average core fuel temperatures are in relatively good agreement, all of them located within a 25 °C width interval. The higher fuel temperature in SAS-SFR (2) calculation may partly be due to higher fuel porosity (5% instead of 4.5%, inducing a reduction of fuel conductivity of 1.5%). Additionally it is to be mentioned that the differences in the values for the total pressure drop indicates that the differences between the two SAS-SFR calculations are due to different assumptions of the inlet pressure drop orificing. In case of the SAS-SFR (1) calculation there is practically no inlet orificing simulated while the inlet orificing in case of the SAS-SFR (2) calculation seem to amount to about 0.5 bar in case of channel 5. This difference could explain some of the differences in the boiling region development especially the initial phase of the recovery of single phase flow conditions.

Temperature axial profiles for every individual channel group were compared between ASTEC-Na and SAS-SFR (1) in addition to the temperatures averaged over the core. The temperatures used for comparison were inner and outer fuel temperatures, averaged fuel temperature, inner cladding temperature and sodium temperature. Examples of temperature axial profiles for channel group 5 are shown in Figs. 6 and 7.

Table 5 Comparison of steady-state values.

	Unit	SAS-SFR (1)	SAS-SFR (2)	ASTEC-Na
Total core pressure drop	[bar]	4.80	5.23	5.28
Total core mass flow rate	[kg/s]	18741.10	18775.60	18906.50
Mean Na core outlet temperature	[°C]	544.98	545.00	545.00
Avg. core fuel temperature	[°C]	1202.68	1228.18	1203.32
Avg. core cladding temperature	[°C]	484.62	484.62	485.78

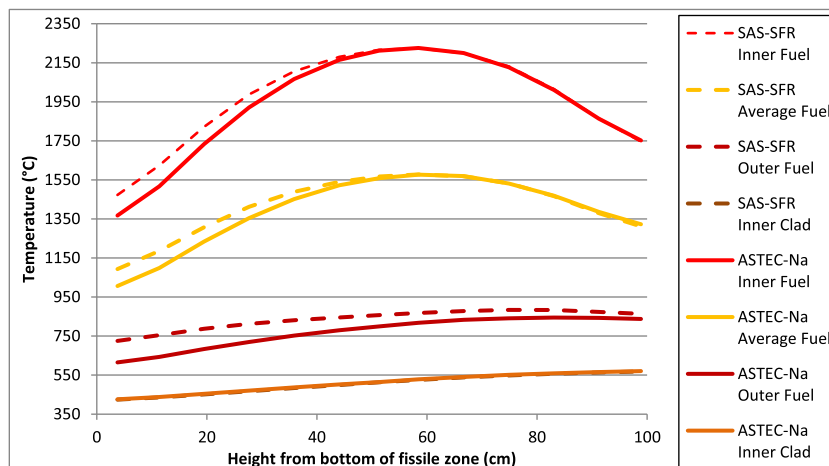


Fig. 6. Comparison of SAS-SFR (1) and ASTEC-Na axial fuel temperature profiles for channel group 5.

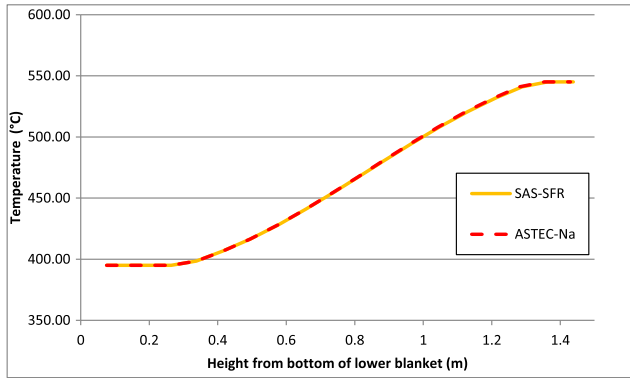


Fig. 7. Comparison of SAS-SFR (1) and ASTEC-Na sodium axial temperature profiles for channel group 5.

The fuel and cladding temperatures in both ASTEC-Na and SAS-SFR (1) simulations are in a relatively good agreement above axial midpoint of the fissile zone, where the difference is below 1%. The reason why the discrepancy on fuel outer temperature does not propagate to fuel inner temperature the same way along the fissile height is not clear. One explanation could be that fuel conductivity evolution temperature is not monotonous but reaches a minimum around 1700 K. For high temperatures, a discrepancy on fuel temperature tends to be counter-balanced by fuel conductivity evolution, whereas it is amplified for low temperatures. Other phenomena, like different fuel pellet restructuring could also be involved (different evolution of fuel inner or outer radius along fissile height).

Higher discrepancies (~ 100 K) can be seen in a lower part of the pin (up to 50 cm from the bottom of lower blanket) for the inner, outer and average fuel temperatures, resulting in up to 8% difference. Significant difference can be observed in outer fuel temperature (varying from 14% to 3% in the lower part of fissile), where SAS-SFR (1) temperature is higher. Significant temperature discrepancy in the lower part can be attributed to the differences in the axially dependent gap heat transfer coefficient being dominantly different due to different assumptions/calculated results on the gap conditions dependent on axial height. This then results in differences of the outer fuel temperature which propagate inwards up to the inner fuel temperature.

Temperature profiles for other channel groups are very similar to the ones of group 5, i.e. all the temperatures are in a relatively good agreement except outer fuel temperatures which is in ASTEC-Na lower compared to SAS-SFR (1).

Finally, sodium axial temperature profiles (Fig. 7) are almost identical in both models, with the temperature difference not exceeding 0.1%.

In both codes inlet and outlet temperatures as well as the total mass flow rate over the core are very close. During steady-state some flow adjustments among different SA groups have been per-

Table 6

Mass flow rates per SA in each channel group, kg/s.

Channel Group	SAS-SFR (1)	SAS-SFR (2)	ASTEC-Na
1	34.85	34.86	35.26
2	36.97	36.96	37.39
3	39.67	39.69	39.85
4	42.10	42.11	42.27
5	57.86	57.75	56.65
6	54.37	54.29	54.79
7	49.02	48.98	49.24
8	41.58	41.48	41.81
9	35.72	35.65	35.89
10	28.25	28.25	28.34

formed to ensure same 150 °C temperature increase along fissile column in all the SA groups. Before transient it was important to check the sodium mass flow rates in different SA groups to ensure that there are no significant discrepancies between the models. Steady-state results of mass flow rates in each of the channel group (per SA) are shown in Table 6.

From the Table 6 it can be seen that the mass flow rates are distributed among channel groups consistently and they are in a good agreement.

As the steady-state conditions are relatively close to each other, the transient simulations start with similar conditions and further deviations in the predicted behaviour of the core are not linked to discrepancies in the initial conditions.

5.2. ULOF transient

The ULOF transient starts at $t=0$ s with the initiation of sodium mass flow coast down at nominal power. The phase I of the transient lasts until around 30 s of transient, when the boiling conditions of the coolant in channel group 5 are reached. For ASTEC-Na onset of boiling occurs at 31.29 s, SAS-SFR (1) at 30.01 s and SAS-SFR (2) at 30.55 s.

The reactor power evolution during the phase I of the transient calculated by two SAS-SFR models and ASTEC-Na (respectively using LOCAL and LOCALM models) is shown in Fig. 8. SAS-SFR (1) and SAS-SFR (2) predictions are in a very good agreement during first 10 s of the transient, but later the results slightly diverge with a maximum difference of about 8% observed at the very end of the phase I. One of the potential causes for this difference could be use of higher fuel porosity in SAS-SFR (2) model (5% instead of 4.5% in other calculations) resulting in higher fuel temperatures and affecting fuel axial expansion reactivity feedback or to slight difference in the boundary conditions. In particular, different approximations are made for pressure boundary where the evolution of inlet pressure is imposed thanks to a time table, and a linear interpolation is performed for times between two input points. As shown in Table 7, the points are coarser in SAS-SFR (1) than in SAS-SFR (2) and this also explains the oscillatory behaviour where oscillations in SAS-SFR (2) calculation are much smaller compared to SAS-SFR (1)'s especially in the range 16–30 s.

Two calculations have been performed using ASTEC-Na for the transient phase I – using temperature variation based neutronics feedback model LOCAL and mass variation based LOCALM. RIA models have been activated for the ASTEC-Na calculation using LOCALM model. The reactor power and total reactivity feedback evolutions calculated by ASTEC-Na LOCAL are in a very good agree-

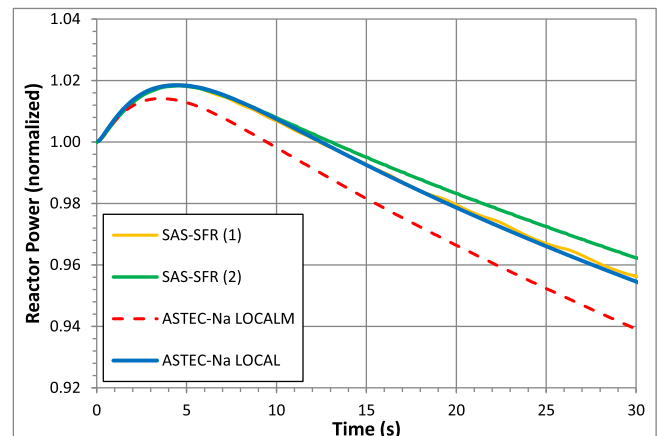


Fig. 8. Power evolution in the first phase of the transient.

Table 7

Pressure boundary.

SAS-SFR (1)	0.0	0.7	1.65	2.5	3.5	4.5	5.5	7.0	8.5	10	11.5	13	14.5	16	19	22	26	30	35	40	
SAS-SFR (2)	$\Delta t = 0.5$ s between $t = 0$ and $t = 2.5$ s and $\Delta t = 1$ s between $t = 2.5$ and $t = 30.5$ s.																				

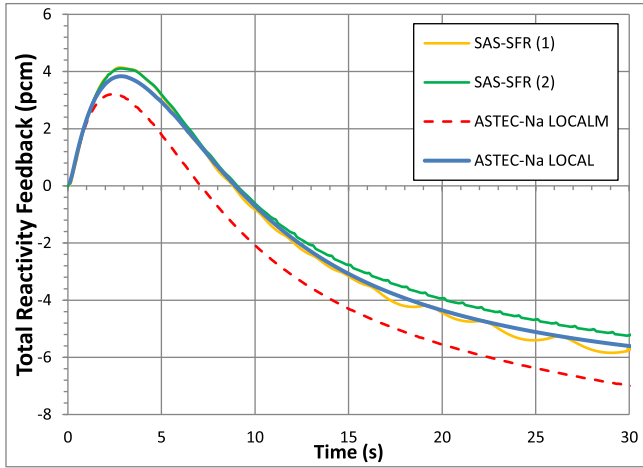


Fig. 9. Total reactivity evolution in the first phase of the transient.

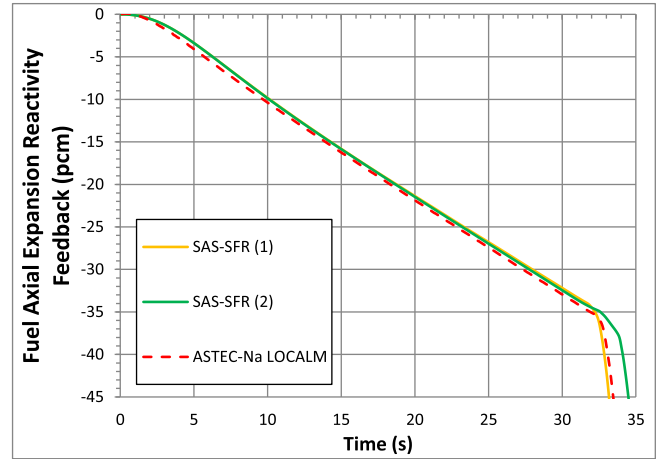


Fig. 12. Fuel axial expansion reactivity feedback.

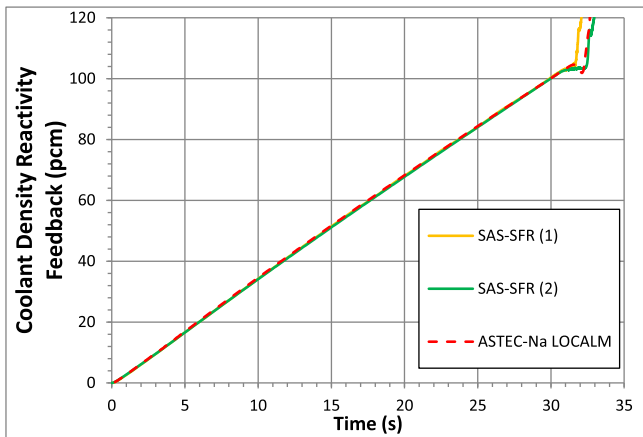


Fig. 10. Coolant density reactivity feedback.

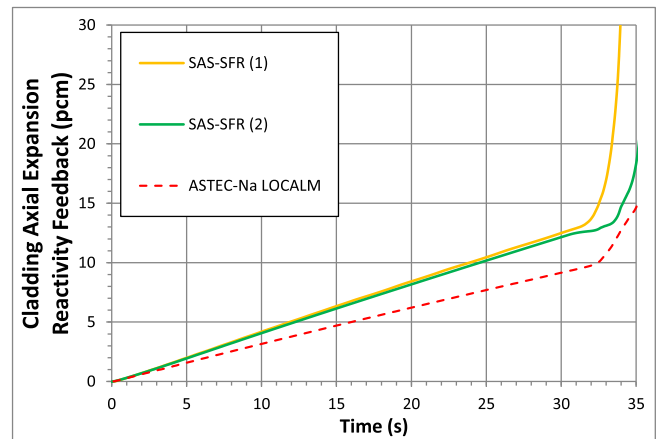


Fig. 13. Cladding axial expansion reactivity feedback.

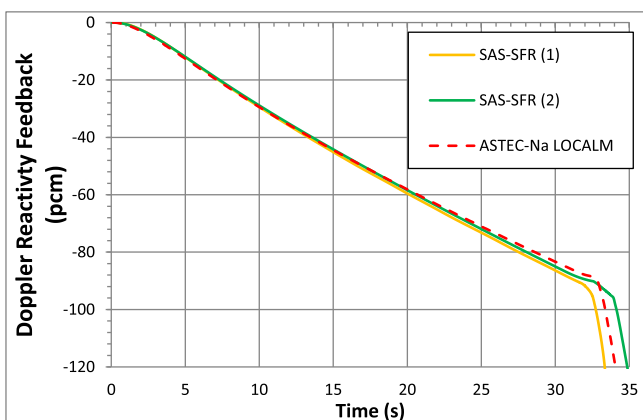


Fig. 11. Doppler reactivity feedback.

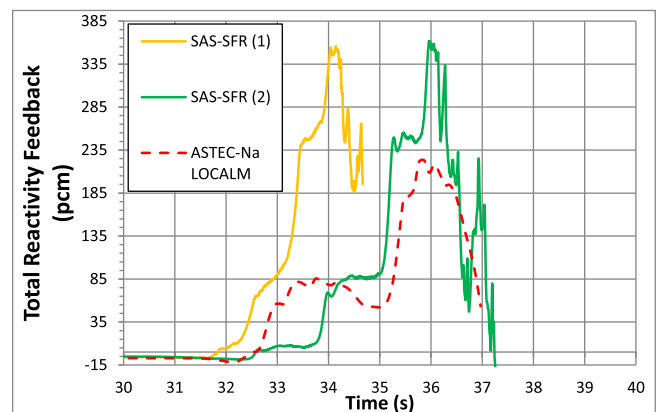


Fig. 14. Total reactivity feedback in the second phase of the transient.

ment with SAS-SFR (1) calculations, while mass variation based model LOCALM calculates a lower power peak due to its slightly lower total reactivity feedback (Fig. 9). The calculated reactivity feedback difference between LOCALM and results obtained by SAS-SFR is within 2% range. LOCAL model better predicts power and reactivity feedback evolutions due to use of temperature variation based reactivity feedback evolution. As a result of this the LOCAL model is less sensitive to differences in physical material properties among different codes resulting in slightly different physical behaviour (e.g. fuel/cladding axial expansion). However, it should be noted that only LOCALM model is suitable for neutron physics feedback reactivity calculations after boiling onset and in case of molten fuel motion, while LOCAL can be used only during phase I calculations (up to the boiling onset).

Because of significant differences how the fuel and cladding expansion reactivity feedbacks are calculated in ASTEC-Na LOCAL model compared to other models – it is not possible to directly compare individual reactivity feedbacks calculated using LOCAL against the ones of ASTEC-Na LOCALM or SAS-SFR. Further comparison in this paper will only consider results calculated by using ASTEC-Na LOCALM model.

By analysing the individual reactivity feedbacks, it appears that ASTEC-Na predicts similar evolutions of the coolant density and Doppler reactivity feedbacks (Figs. 10 and 11) while respectively slightly over-predicts the contribution of the fuel axial expansion (Fig. 12) and under-predicts that of the cladding axial expansion (Fig. 13) to the total reactivity feedback. Overestimation of the fuel axial expansion reactivity feedback from the very first seconds of the transient is the main cause leading to the underestimation of total reactivity feedback and power during first seconds. Given the good agreement of ASTEC-Na results using the LOCAL reactivity feedback model (based on temperature), the differences observed in reactor power and total reactivity feedback evolution calculated by SAS-SFR and ASTEC-Na when using the LOCALM model is explained by the difference in fuel and cladding axial expansion calculations between the two codes with similar material temperature evolution.

Overestimation of fuel axial expansion reactivity feedback is mainly due to deficiencies in ASTEC-Na RIA model. Some improvements with the release of ASTEC-Na v2.1 have been made, however there's still some improvement needed in estimation of fuel axial expansion. Underestimation of cladding axial expansion reactivity feedback most likely is the combination of discrepancies among ASTEC-Na and SAS-SFR in cladding material properties as well as differences in physical models used. From Figs. 12 and 13 it can be seen that underestimation of cladding axial expansion is the one important factor leading to the lower total reactivity feedback values in ASTEC-Na.

From Fig. 9 it can be seen that ASTEC-Na calculations in general correctly follows expected total reactivity evolution in the first phase of the transient. Typically, the reactor power initially increases due to sodium reactivity feedback and when other reactivity feedbacks become effective, the power starts to decrease. Before onset of coolant boiling the net reactivity remains negative. This phase is characterized by a quick single phase coolant heat-up which leads to coolant boiling. The boiling onset and the subsequent cladding dry-out, melting and relocation introduce a positive reactivity feedback which results in a power excursion. The power increase accelerates fuel melting leading to fuel pin break-up and fuel relocation resulting in negative reactivity insertion reducing net reactivity and power at the entry to the transition phase.

The calculation performed with ASTEC-Na beyond the boiling onset and using LOCALM model shows the capability of the code to compute boiling conditions together with a great power excursion due to the large positive reactivity insertion (Figs. 14 and 15). The fuel/cladding thermo-mechanical relocation models in ASTEC-

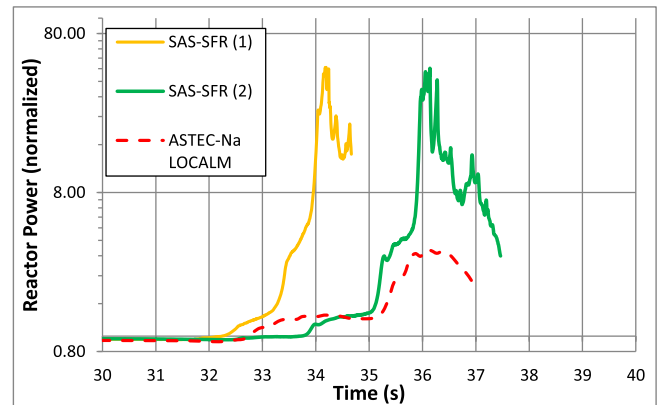


Fig. 15. Reactor power evolution in the second phase of the transient.

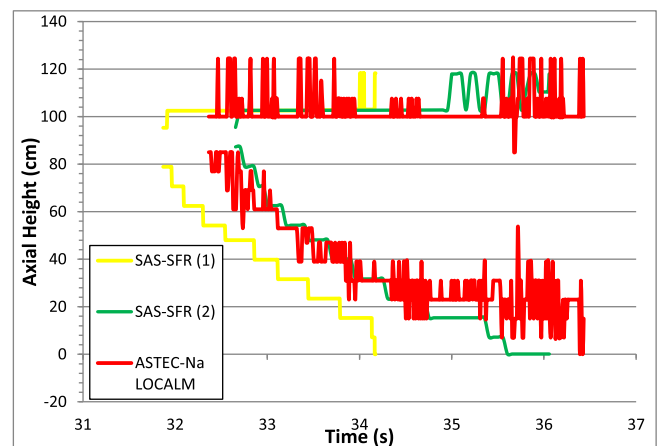


Fig. 16. Channel 5 cladding dry-out front progression.

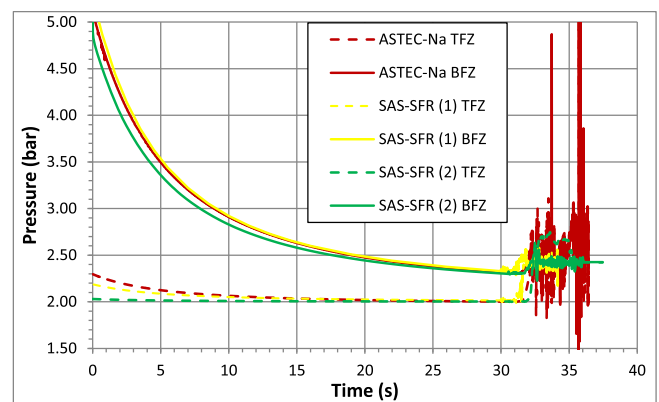


Fig. 17. Channel 5 pressure evolution at BFZ and TFZ.

Na are still under development and only in-pin fuel relocation model is ready. This impedes to assess the maximum power/reactivity feedback peak reached during the transient after fuel or cladding melting and relocation start (Fig. 15). However, the overall behaviour is qualitatively in agreement among the codes. The different onset of reactivity increase and consequent start of the power excursion (Fig. 14) is mainly due to the different times of boiling onset and partly due to differences in the calculated void propagation (Figs. 16–18).

The cladding dry-out progression for channel 5 (Fig. 16) has been extracted from ASTEC-Na results indirectly – a void coeffi-

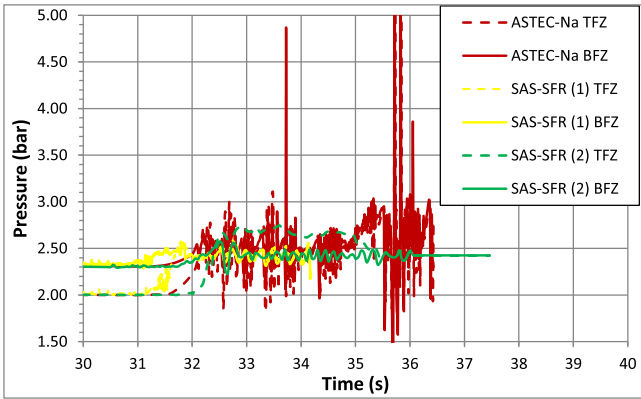


Fig. 18. Channel 5 pressure evolution at BFZ and TFZ for the boiling phase.

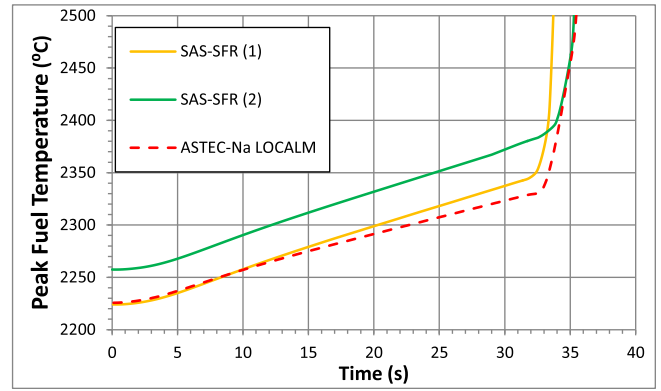


Fig. 21. Channel 5 peak fuel temperature.

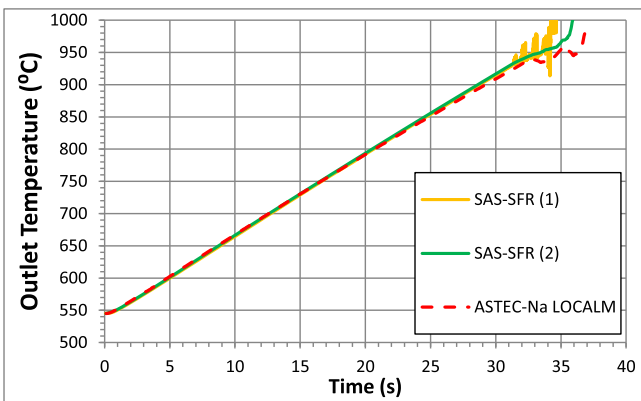


Fig. 19. Channel 5 outlet sodium temperature.

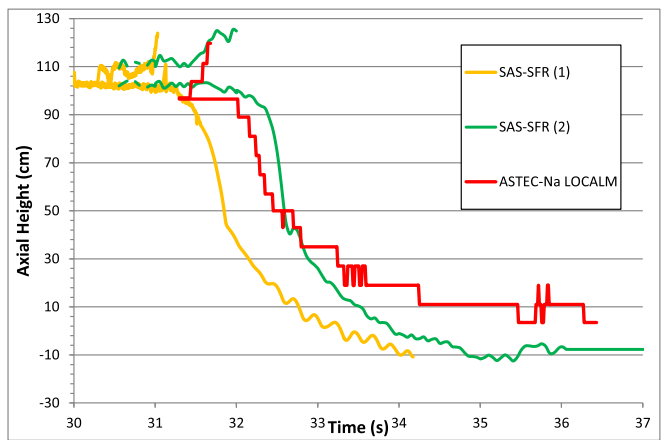


Fig. 22. Channel 5 sodium two-phase interface. (For interpretation of the references to colour in this figure legend, the reader is referred to the web version of this article.)

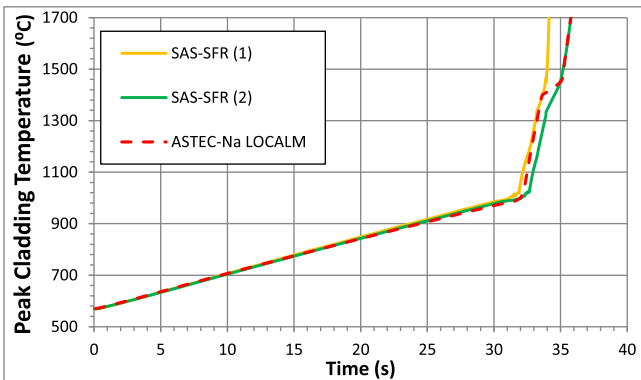


Fig. 20. Channel 5 peak cladding temperature.

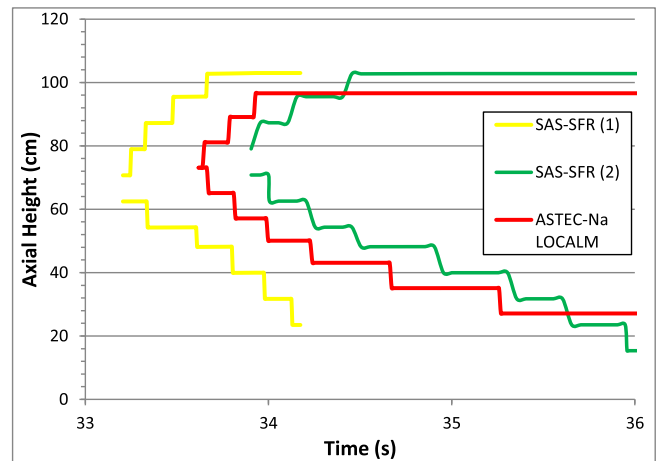


Fig. 23. Channel 5 cladding melt progression.

cient threshold level of 0.9998 in a sodium mesh has been used to presume cladding dry-out.

Apart from the start of cladding dry-out, ASTEC-Na and SAS-SFR calculate a similar evolution of its progression both towards the top and bottom of the fuel assembly. There is a small shift between different results due to different times of boiling onset and slight differences in the boiling front propagation kinetics.

After the onset of boiling, the results show first a small decrease of total reactivity calculated by all codes and then the sharp increase due to the coolant feedback (Fig. 14). The small reactivity decrease after boiling is due to the negative contribution coming from the voiding of the upper part of the fuel pin.

In this calculation, the maximum positive total reactivity shown by SAS-SFR is over 340 pcm, and then the negative fuel relocation

feedback plays the major role in the reduction of the total reactivity. This results in a total power excursion of about 50 times the nominal power. The difference in the boiling dynamics of the two SAS SFR calculations most probably is due to the different assumptions on the inlet orificing established at the steady-state representation. Fig. 17 shows the pressure evolution in channel 5 at bottom fertile zone (BFZ) and top fertile zone (TFZ) for the whole transient. Fig. 18 focuses on the pressure behaviour in the second phase of the transient.

The temperature evolutions of sodium, cladding and fuel are generally in good agreement among the codes during the first phase of the transient (Figs. 19–21). ASTEC-Na computes a slightly lower sodium outlet temperature at the end of phase I, given the lower power evolution. A difference in the initial value of the peak fuel temperature is observed for SAS-SFR (2) calculation, consistent to what was observed on average core fuel temperature (Table 5).

However no significant differences are observed in the temperature gradient calculated with ASTEC-Na compared to results of other codes. Discrepancies in the peak fuel temperature evolution are mainly due to lower power calculated by ASTEC-Na and discrepancies in the temperature evolution during the phase II of the transient are due to the different time when the onset of boiling is calculated by the different codes.

All codes predict the initial position of the boiling front at the top of the fissile zone (Fig. 22). The front then progresses in opposite directions towards the top and the bottom of the fuel assembly showing also a good agreement among the codes. In ASTEC-Na lower boiling front is in a rather good agreement with SAS-SFR predictions. However, the lower boiling front does not extend downward to the same degree as in the SAS-SFR calculations. This most probably is due to the lower power values calculated in the ASTEC-Na calculation. In addition one important factor affecting boiling front prediction in ASTEC-Na is model meshing. Within JASMIN WP2.1 (devoted to sodium thermal-hydraulics model) it has been demonstrated that use of different meshing (fine vs rough) significantly affects boiling front prediction results (Flores y Flores et al., 2016). The oscillations of the yellow curve in Fig. 22 are a plotting error in case of the disappearance of bubbles i.e. return to single phase conditions This is calculated during the first half second in case of the SAS-SFR (1) calculation. The reason for this behaviour is the inlet orificing established very small in this calculation. The explanation for the different timing of the behaviour of the lower void front in SAS-SFR calculations is the very small inlet orificing established.

With regards to the upper boiling front predictions – all the models were based on the simplified reactor core layout (Fig. 3) and as a result of this, prediction of the upper boiling front is limited to the top of the upper gas plena (approx. 123 cm from bottom of fissile). As the main goal of the benchmark was to test new neutron physics model features but not to predict boiling front – more detailed model was not considered feasible.

As with the cladding dry-out front similar results were obtained for cladding melt progression (Fig. 23). Despite the shift in time due to different cladding melting onset times, the cladding melt progression is consistent between ASTEC-Na and SAS-SFR.

6. Conclusions

Based on the Point Kinetics model, the ASTEC-Na neutron physics model provides actually two different methods to compute the reactivity feedbacks: one model (called LOCAL) uses coefficients related to temperature (pcm/K), the other model (LOCALM) is based on mass variation and allows extending the scope of the ASTEC-Na neutronics model to post boiling onset analysis. More specifically, the LOCALM model is able to predict reactivity evolution resulting from sodium boiling, and molten fuel in-pin relocation.

The results show that the LOCALM is correctly implemented and allows ASTEC-Na to calculate the neutron physics feedback and associated power response. Main discrepancies between ASTEC-Na and SAS-SFR benchmark results are associated with the different material expansion models used, different meshing systems as well as different fuel thermo-mechanical models that might lead to different gap conductance and different conditions

for calculating fuel thermal conductivity. Some numerical problems still exist in handling sharp power excursions in the thermal-hydraulic model CESAR, but those are not directly related to the neutron physics model.

Further ASTEC-Na developments are needed allowing modelling of molten fuel and cladding relocation. Currently only in-pin molten fuel movements are simulated, however this is not sufficient for simulation of slow power excursions under dry-out conditions. Actually, in sharp power excursion, in-pin fuel motion can play a major role as in-pin pressure axial gradient will be high, whereas in dry-out conditions and slow power increase, no internal pressure peak and in-pin fuel motion is less likely to be significant. For ULOF scenarios, in-pin fuel relocation is anyhow hardly of importance because early fuel pin break-up limits the time window for which this effect can become relevant.

The Point Kinetics model developed is very valuable for understanding the phenomena leading to reactivity changes as this latter is decomposed in several contributions which can be hard to guess when material relocation starts. The possibility offered by the model to make the sets of reactivity feedback coefficients evolve during the transient is a great strength which will need to be confronted against codes with space-time kinetics, as well as its ability to deal with heterogeneous core designs.

Acknowledgements

This work was financed by the JASMIN project No. 295803 within the 7th Framework Programme of the European Commission in the Topic Fission-2011-2.2.1 “Support for ESNII”.

The authors thank Dankward Struwe and Werner Pfrang for the technical support provided in the preparation of this work.

References

- Bessiron, V., 1998. Implementation of New Sodium Equations of State in SAS4A. Note Technique SEMAR 98/26 IPSN.
- Blanchet, D., Buiron, L., 2009. CP ESFR Working Horses Core Concept Definition, Deliverable CP ESFR SP2.1.2.D1.
- Cahalan, J.E., Tentner, A.M., Morris, E.E., 1994. Advanced LMR Safety Analysis Capabilities in the SASSYS-1 and SAS4A Computer Codes. In: Proceedings of the International Topical Meeting on Advanced Reactor Safety, vol. 2, Pittsburgh, PA, 1994, pp. 1038–1045.
- Cloarec, L., Moal, A., 2012. Documentation for ASTEC-Na RIA model. IRSN report PSN-RES/SAG/2012-00331.
- Dagan, R., Sanchez, V., Travleev, A., 2004. KAPROS-E: Modular Program System for Nuclear Reactor Analysis, Status and Results of Selected Applications, C.H.M. Broeders, Jahrestagung Kerntechnik, Düsseldorf, May 25–27.
- Fiorini, G.L., Vasile, A., 2011. European Commission – 7th framework programme: the collaborative project on European sodium fast reactor (CP ESFR). Nucl. Eng. Des. 241 (9), 346.
- Flores y Flores, A. et al., 2016. Analysis of ASTEC-Na capabilities for simulating a loss of flow CABRI experiment. Ann. Nucl. Energy 94, 175–188.
- Genshiyoku, A., Kiban, K., 2011. A SAS4A Study on the ULOF Initiating Phase Energetics of the Fast Breeder Reactor (FBR). JNES/FBRG10-004. Japan Nuclear Energy Safety Organization (JNES). Feb. 2011.
- Girault, N., Cloarec, L., et al., 2015. On-going activities in the European JASMIN project for the development and validation of ASTEC-Na safety simulation code. In: Proceedings of ICAPP 2015, May 03-06, 2015, Nice, France.
- Girault, N., Van Dorselaere, J.P., et al., 2013. The European Jasmin project for the development of a new safety simulation code, ASTEC-Na, for Na-cooled fast neutron reactors. In: 2013 International Congress on Advances in Nuclear Power Plants & 28th KAIF/KNS Annual Conference, Jeju Island, Korea.
- Hill, D.J., 1985. SAS4A Validation and Analysis of In Pile Experiments for Slow Ramp TOP's. In: Proceedings of the International Topical Meeting on Fast Reactor Safety, American Nuclear Society, Knoxville, TN, April 21–25, 1985.
- Imke, U., Struwe, D., et al., 1994. Status of the SAS4A-code development for consequence analysis of core disruptive accidents. In: Proceedings of an International Topical Meeting. Sodium Cooled Fast Reactor Safety. 2-232. Obninsk, Russia, (October 1994)
- KANEXT description <http://chmblh.eu/kaprose.php>.
- Kruessmann, R. et al., 2015. Assessment of SFR reactor safety issues: Part II: analysis results of ULOF transients imposed on a variety of different innovative core designs with SAS-SFR. Nucl. Eng. Des. 285, 263–283.

- Moal, A., Georgenthum, V., Marchand, O., 2014. SCANAIR: a transient fuel performance code. Part One: general modelling description. *Nucl. Eng. Des.* 280, 150–171.
- Papin, J. et al., 1996. French Studies on high-burnup fuel transient behavior under RIA conditions. *Nucl. Saf.* 37, 289–327.
- Perez-Martin, S., Pfrang, W., 2015. Analysis of the E7 CABRI experiment, a structured top transient in restrained conditions with SAS-SFR code. In: Proceedings of ICONE-23, 3th International Conference on Nuclear Engineering, May 17–21, 2015, Chiba (Japan).
- Perez-Martin, S., Pfrang, W., 2016. Analysis of high burn-up annular fuel pin behavior under a cabri transient over power with the SAS-SFR Code. In: Proceedings ICAPP 2016 San Francisco (USA).
- Rineiski, A., et al., 2011. Synthesis of options to optimize feedback, 2012. Deliverable CP ESFR SP2.1.3.D1.
- The JASMIN FP7 project, <http://www.jasmin-fp7.eu>.
- Wider H.U. et al., 1982. Status and Validation of the SAS4A Accident Analysis Code System. In: Proceedings of the LMFBR Safety Topical Meeting, European Nuclear Society, Lyon, France, July 19 23, 1982.